

# The Morphology of the Expanding Ejecta of V2491 Cygni (2008 N.2)

V. A. R. M. Ribeiro,<sup>1\*</sup> M. J. Darnley,<sup>1</sup> M. F. Bode,<sup>1</sup> U. Munari,<sup>2,3</sup>  
D. J. Harman,<sup>1</sup> I. A. Steele<sup>1</sup> and J. Meaburn<sup>4</sup>

<sup>1</sup> *Astrophysics Research Institute, Liverpool John Moores University, Twelve Quays House, Egerton Wharf, Birkenhead, CH41 1LD*

<sup>2</sup> *INAF Astronomical Observatory of Padova, via dell'Osservatorio, 36012 Asiago (VI), Italy*

<sup>3</sup> *ANS Collaboration, c/o Astronomical Observatory, 36012 Asiago (VI), Italy*

<sup>4</sup> *Jodrell Bank Centre for Astrophysics, University of Manchester, Oxford Road, Manchester, M13 9PL*

Accepted 2010 November 8. Received 2010 November 8; in original form 2010 September 22

## ABSTRACT

Determining the evolution of the ejecta morphology of novae provides valuable information on the shaping mechanisms in operation at early stages of the nova outburst. Understanding such mechanisms has implications for studies of shaping for example in proto-Planetary Nebulae. Here we perform morpho-kinematical studies of V2491 Cyg using spectral data to determine the likely structure of the ejecta and its relationship to the central system and shaping mechanisms. We use *SHAPE* to model different morphologies and retrieve their spectra. These synthetic spectra are compared with observed spectra to determine the most likely morphology giving rise to them, including system inclination and expansion velocity of the nova ejecta. We find the best fit remnant morphology to be that of polar blobs and an equatorial ring with an implied inclination of  $80_{-12}^{+3}$  degrees and an maximum expansion velocity of the polar blobs of  $3100_{-100}^{+200}$  km s<sup>-1</sup> and for the equatorial ring  $2700_{-100}^{+200}$  km s<sup>-1</sup>. This inclination would suggest that we should observe eclipses which will enable us to determine more precisely important parameters of the central binary. We also note that the amplitude of the outburst is more akin to the found in recurrent nova systems.

**Key words:** line: profiles – stars: novae – stars: individual: V2491 Cyg

## 1 INTRODUCTION

A classical nova (CN) outburst occurs in an interacting binary system comprising a main-sequence or evolved star (the secondary), which fills its Roche Lobe, and a white dwarf (WD; the primary). Matter transferred from the secondary to the WD builds up on the surface. Once extensive CNO cycle nuclear burning commences under these degenerate conditions, a thermonuclear runaway occurs ejecting  $\sim 10^{-5}$ – $10^{-4}$   $M_{\odot}$  of matter from the WD surface with velocities from hundreds to thousands of km s<sup>-1</sup> (see, e.g. Bode & Evans 2008; Bode 2010, and references therein). A related sub-class of CNe are the recurrent novae (RNe), which unlike CNe, recur on time-scales of order tens of years. Such a short recurrence time-scale is usually attributed to a high mass WD, probably close to the Chandrasekhar limit, together with a high accretion rate (Starrfield et al. 1985; Yaron et al. 2005).

Nova Cygni 2008 N.2 (hereafter, V2491 Cyg) was discovered on 2008 April 10.8 UT (taken as  $t = 0$ ) at about 7.7 mag on unfiltered CCD frames (Nakano et al. 2008) and its nature confirmed spectrometrically yielding velocities of  $\sim 4500$  km s<sup>-1</sup> ( $H\alpha$  FWHM, Ayani & Matsumoto 2008). Henden & Munari (2008) identified USNO-B1.0 1223-042965 as the likely progenitor sys-

tem (within 0.9 arc seconds of V2491 Cyg). An archival search by Jurdana-Sepic & Munari (2008) of the Asiago Schmidt telescope images of the progenitor collected over the period 1970-1986 showed no previous outburst. Munari et al. (2010b) have provided a detailed study of the photometric and spectrometric evolution of V2491 Cyg, including a photo-ionization analysis of the ejecta and their chemical abundances. They derived the reddening for V2491 Cyg of  $E(B - V) = 0.23 \pm 0.01$ , a distance of 14 kpc, and  $V = 17.9$ ,  $R_c = 17.5$ ,  $I_c = 17.1$  for the progenitor in quiescence.

In Fig. 1 we show the light curve for the first 50 days after outburst from the AAVSO<sup>1</sup>. A rapid decline is observed for the first 10 days after outburst and then a sudden rebrightening peaking around day 15. It is not fully understood why this rebrightening should happen. For example, Hachisu & Kato (2009) have modelled the rebrightening by introducing magnetic activity as an additional energy source to nuclear burning. Although, a magnetic WD has a spin closely related to the binary orbital period (King et al. 1990), taken previously by several authors as 0.0958 days (Baklanov et al. 2008), but there is no observed evidence of a short periodicity in the X-rays related to the orbital period (Ibarra et al. 2009; Page et al. 2010) and generally polars are weak X-ray sources (King & Watson 1987). It is also noteworthy

\* E-mail: var@astro.livjm.ac.uk

<sup>1</sup> See <http://www.aavso.org/>

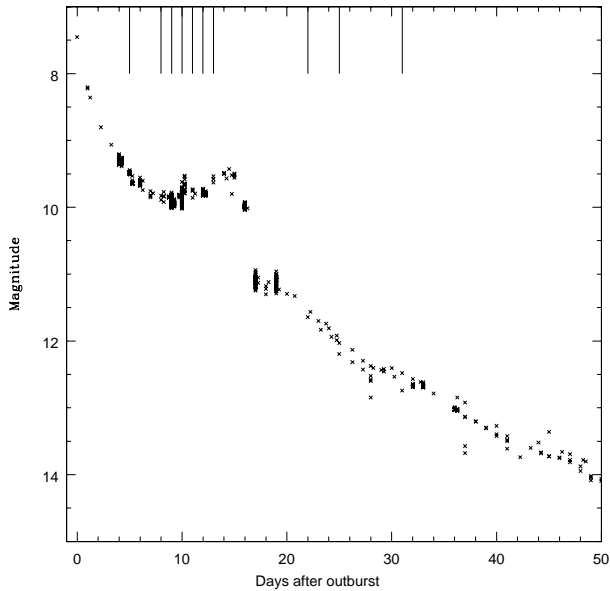


**Figure 1.** Optical light curve for V2491 Cyg from AAVSO data. The vertical lines are days where data were taken with the Meaburn Spectrograph on the 2-meter robotic Liverpool Telescope.

that A. Baklanov (private communication) is not confident that the above period is related to the orbital period of the system, a matter that is addressed in Darnley et al. (2010).

V2491 Cyg is of particular interest because it was detected as an X-ray source pre-outburst (Ibarra & Kuulkers 2008; Ibarra et al. 2008, 2009). This is only the second CN to be detected in X-rays pre-outburst (after V2487 Ophiuchi, Hernanz & Sala 2002). V2487 Oph was originally suggested to be a RN because of its rapid decline in the optical domain and the presence of a plateau phase during decline (see e.g., Hachisu et al. 2002; Hernanz & Sala 2002). V2487 Oph’s true recurrent nature came to light only after a search of the Harvard College Observatory archival photographic collection revealed an outburst on 1900 June 20 (Pagnotta et al. 2009). They used two methods to determine a recurrence timescale of order  $\sim 20$  years, a Monte Carlo simulation to calculate the probability that a given recurrence timescale would produce exactly two discovered eruptions and by directly estimating the most likely number of eruptions. Furthermore, V2491 Cyg has very similar properties to the suggested extragalactic RN M31N 2007-12b, which was shown to have similar magnitude and colour to the RN RS Oph at quiescence (Bode et al. 2009). On the other hand, Ibarra et al. (2009) derived 0.2–10 keV X-ray luminosities ranging from  $10^{34}$ – $4 \times 10^{35}$  erg s $^{-1}$  implying inter-outburst mass accretion rates in the range of  $10^{-9}$  to  $10^{-8}$   $M_{\odot}$  yr $^{-1}$  for a 1  $M_{\odot}$  WD. Such low values for the accretion rate would imply a recurrence timescale of  $\geq 100$  yrs (Yaron et al. 2005; Ibarra et al. 2009; Page et al. 2010). However, a higher WD mass will reduce the recurrence time.

Post-outburst *Swift* observations of V2491 Cyg showed a clearly detected X-ray source, although the count rate was almost an order of magnitude fainter than during pre-outburst observations (Page et al. 2010). The post-outburst observations showed three distinct phases: first a hard X-ray emission phase, then a super-soft source (SSS) phase and finally the decline of the SSS with the

hard component again becoming prominent, since it fades much less rapidly than the SSS emission (Page et al. 2010).

For decades it has been known that spectral line profiles contain a great deal of information about the expanding remnant of a nova outburst (e.g., Hutchings 1972). Here we use spectrometric data to constrain the structure and velocity field for the expanding remnant of V2491 Cyg. In Section 2, we describe our observations and data reduction methodology. The results are presented in Section 3 and then modelled in Section 4. In Section 5 we present the results of the modelling and in Section 6 we discuss the implications of the results.

## 2 OBSERVATIONS AND DATA REDUCTION

Optical spectra of V2491 Cyg were obtained with the Meaburn Spectrograph (a thermocoiled, Apogee AP7p 512 $\times$ 512 pixel thinned Tektronix array prototype fibre-fed robotic spectrograph, now superseded by FRODOSpec) on the 2-metre robotic Liverpool Telescope (LT; Steele et al. 2004) sited at the Observatorio del Roque de Los Muchachos on the Canary Island of La Palma, Spain. The spectrograph was fed using a close-packed fibre bundle input array, consisting of  $49 \times 0.8''$  diameter fibres which were reformatted as a slit with the fibres in random order.

The observations were carried out over several epochs from  $t = 5$  days (2008 April 16) to 31 days (2008 May 12) post-outburst. The log of spectrometric observations is shown in Table 1. The spectrograph provided three overlapping fixed grating positions, giving complete wavelength coverage from 3900–8000Å. However, we only use a single grating position (5350–6888Å) with dispersion of 3.00 Å/pix and spectral resolving power  $\sim 350$ . Data reduction was performed through a pipeline that initially performs bias, dark frame and flat field subtraction. With a comparison arc spectrum, a third order polynomial 2D wavelength/distortion map was created using the STARLINK Figaro ARC/IARC/ISCRUNCH routines and applied to the object image. Sky subtraction based on identification of non-object areas of the 2D spectrum was then carried out, if significant sky lines were visible, using the Figaro routine POLYSKY. A 1D spectrum was then automatically extracted using the PROFILE and OPTEXTRACT routines. Relative flux corrections were accomplished by using observations of a number of early type Be stars (showing few absorption lines) obtained for a different programme. Absorption lines were patched over and the star’s temperature was chosen following their spectral types (Boehm-Vitense 1981). Using the STARLINK Figaro IRFLUX routine we corrected the spectra for instrumental efficiency/atmospheric absorption. In Fig. 2 we show the computed flux-corrected spectra from  $t = 5$  to 31 days after outburst.

We also obtained spectrometric observations at  $t = 2, 25, 33, 108$  and 477 days after outburst with: (i) the 0.6m telescope of the Schiaparelli observatory in Varese equipped with a multi mode spectrograph and various reflection gratings, (ii) the 3.5m TNG in La Palma and the high resolution spectrograph SARG ( $\Delta\lambda/\lambda = 75000$ ), and (iii) the spectrograph/imager AFOSC on the 1.82m telescope of the Padova Astronomical Observatory in Asiago with wavelength coverage of 6400–7050Å. This is part of the observational monitoring of V2491 Cyg is described by Munari et al. (2010b) to which the reader is addressed for full details about data acquisition and reduction.

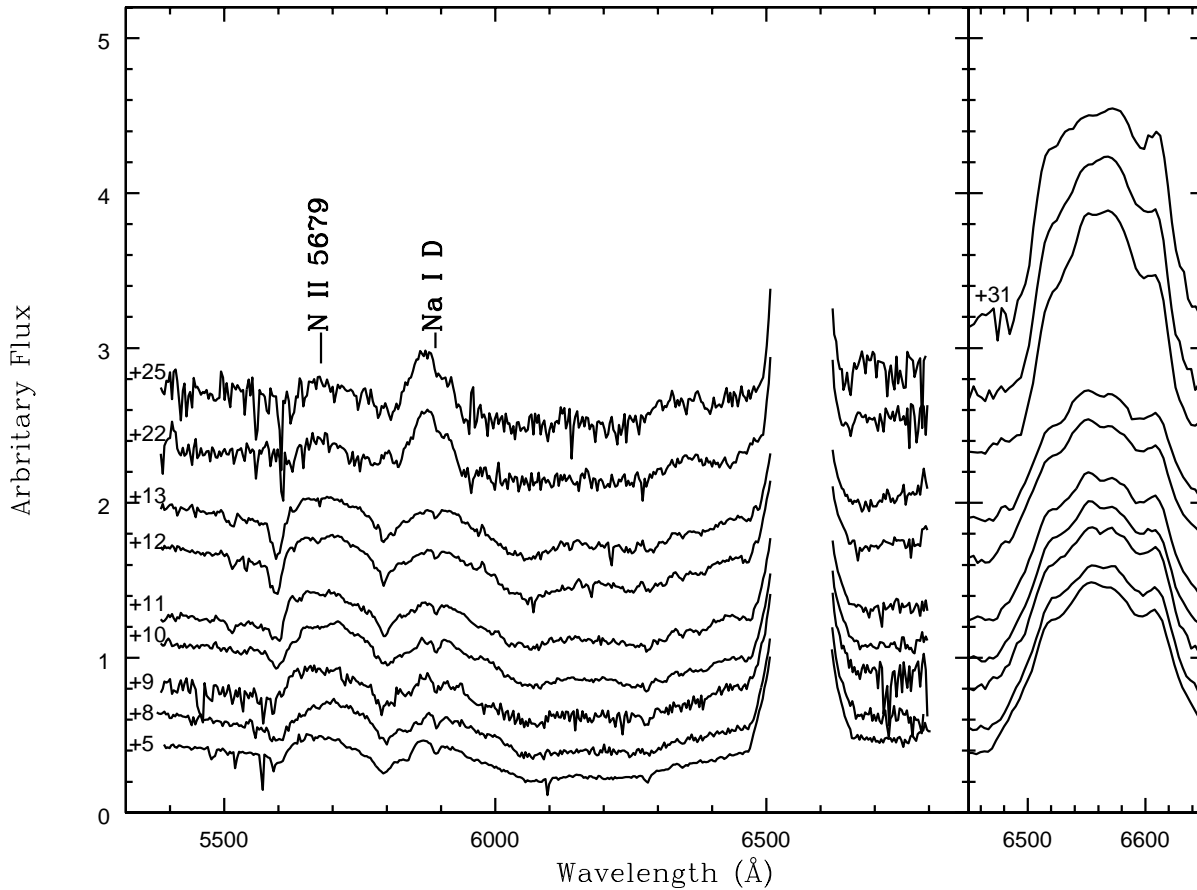


**Figure 2.** Meaburn spectrometric observations of V2491 Cyg during days 5–31 (2008 April 06 to 2008 May 12). The Meaburn spectra have been corrected for instrumental efficiency/atmospheric transmission using Be Star comparison spectra (see text for details). On the left-hand-side we have truncated the H $\alpha$  emission to show more clearly the lower intensity lines. The spectrum on day 31 after outburst was too noisy at this low level, so we only plot the H $\alpha$  line. On the right-hand-side the H $\alpha$  line profiles are shown. The time since outburst (in days) is shown to the left of each spectrum. Cosmic rays have also been removed. The higher resolution (non-Meaburn spectrograph) H $\alpha$  profiles in Table 1 are shown in Fig. 4.

**Table 1.** Log of optical spectral observations of V2491 Cyg.

Date of observation	days after outburst	Exposure time (sec)	Instrument
2008 April 13	2	900.0	Varese-MMS
2008 April 16	5	200.0	Meaburn-LT
2008 April 19	8	200.0	Meaburn-LT
2008 April 20	9	200.0	Meaburn-LT
2008 April 21	10	200.0	Meaburn-LT
2008 April 22	11	200.0	Meaburn-LT
2008 April 23	12	200.0	Meaburn-LT
2008 April 24	13	200.0	Meaburn-LT
2008 April 25	14	300.0	SARG-TNG
2008 May 03	22	600.0	Meaburn-LT
2008 May 06	25	600.0	Meaburn-LT
2008 May 12	31	600.0	Meaburn-LT
2008 May 14	33	1800.0	Varese-MMS
2008 July 27	108	900.0	Asiago-AFOSC

### 3 OBSERVATIONAL RESULTS

We analysed the spectral information first to get an initial estimate of the component parameters before detailed modelling of V2491 Cyg began. The spectra show broad H $\alpha$ , nitrogen (N II 5679Å) and sodium (Na I D) lines (Fig. 2). The spectral monitoring by Munari et al. (2010b) shows that at day +33 after outburst the auroral [N II] 5755 line was still pretty weak, and thus the nebular [N II] 6458, 6584 lines should not yet be perturbing the H $\alpha$  profile. Also evident is a narrowing of the H $\alpha$  line profile from day 22 after outburst, which is after the optical rebrightening. We cannot say why this rebrightening should happen but it is noteworthy that Munari et al. (2010b) also observed a decrease in the equivalent widths of the H $\beta$  line around this time. The N II and Na I lines seen are similar to those seen in the early spectrum of V394 CrA (Williams et al. 1991). However, these lines disappear from the spectrum of V394 CrA 20 days after its 1987 outburst. In the case of V2491 Cyg both are clearly present later after outburst. The N II line, as in V394 CrA, is most likely due to continuum fluorescence from the post-outburst WD radiation.

The line of interest for our detailed analyses is H $\alpha$  because of its strength compared to those of other lines visible in the spectrum.

**Table 2.** Derived radial velocity for each of the 5 components of the H $\alpha$  line in V2491 Cyg (see Fig. 3 and text for details).

Date	days after outburst	Component Radial Velocity (km s <sup>-1</sup> )				
		1	2	3	4	5
2008 April 16	5	-1875±32	-530±34	117±3529	615±64	2028±68
2008 April 19	8	-1860±17	-510±22	112±961	671±61	2085±19
2008 April 20	9	-1899±50	-537±38	98±849	700±28	2088±3
2008 April 21	10	-1828±65	-482±48	99±2529	653±8	1994±53
2008 April 22	11	-1909±76	-531±55	92±1209	687±59	2043±24
2008 April 23	12	-2025±163	-642±93	120±1551	680±87	2072±120
2008 April 24	13	-2054±67	-720±72	90±1341	558±29	2009±65
2008 May 03	22	-1634±47	-610±30	184±29	673±30	2088±26
2008 May 06	25	-1739±218	-716±20	96±33	687±58	2015±44
2008 May 12	31	-1865±92	-822±111	334±91	368±368	2094±5

Furthermore, later in outburst other emission lines are severely blended (Munari et al. 2010b). Using the low resolution Meaburn spectra we initially fit five Gaussian components to the spectra (see Fig. 3). This allows us to derive the individual components' radial velocities and their respective FWHM (see Tables 2 and 3, respectively). There is evidence for velocity symmetry between the faster moving components, 1 and 5. Components 2, 3 and 4 are much harder to constrain, especially component 3 which becomes stronger after rebrightening. We find the displacement of the line profile from the rest wavelength of the H $\alpha$ , using components 1 and 5, to be  $92\pm 36$  km s<sup>-1</sup>.

#### 4 MODELLING

Using SHAPE (Version 3.56, Steffen & López 2006; Steffen et al. 2010)<sup>2</sup> we performed morpho-kinematical studies of V2491 Cyg. Classical nova ejecta have been modelled with various structures (e.g., Hutchings 1972; Solf 1983; Gill & O'Brien 1999). Work by Slavin et al. (1995), later updated by Bode (2002), suggested a relationship between the speed class (in terms of the time for the wind flux to decline 3 magnitudes from peak -  $t_3$ ) and the major to minor axis ratio of the expanding nova shell, where the faster the nova the less the degree of shaping. This relationship works well with CNe (short orbital period systems) and possibly RNe of short orbital period. However, RS Oph, a system with orbital period of 455 days (Kenyon 1994; Fekel et al. 2000; Brandi et al. 2009), at 155 days after outburst showed a deprojected major to minor axial ratio of 3.85 (Ribeiro et al. 2009), which considering its fast optical decline would not agree with the relationship originally found by Slavin et al. (1995). Recent results for V2672 Oph also appear to disagree with this relationship (Munari et al. 2010a). However, we expect that the mechanism for formation of CN and RN shells, especially those RNe with long orbital periods, to be different. For example, systems such as RS Oph have remnants grossly affected by the interaction of ejecta with the pre-existing red-giant wind, which is unique to this sub-group of RNe.

Several mechanisms have been proposed to be involved in the shaping of CN ejecta. These can be identified as that associated with the common-envelope phase during outburst, the presence of a magnetised WD, the spin of the WD and an asymmetric thermonuclear runaway (see e.g., O'Brien & Bode 2008). The most widely accepted model involves the common-envelope phase

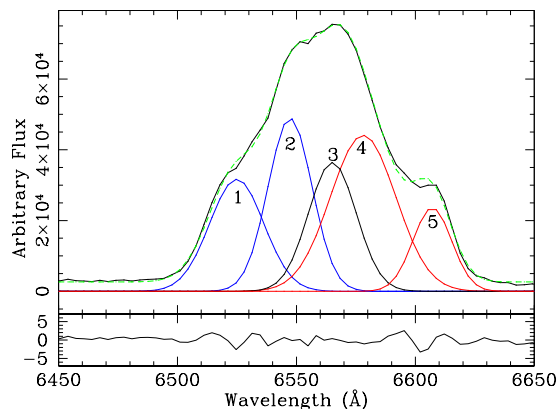


**Figure 3.** Gaussian components best fit to the observed H $\alpha$  line profile for V2491 Cyg on day 25 after outburst. The observed spectrum is shown in black and the combined Gaussian components in dashed green. The colour scheme for the individual Gaussian components are just to separate the different components. The component numbers, 1 through 5, are in increasing wavelength of the peak. Also shown are the residuals to the overall fit. The results for the derived radial velocities of each peak and FWHM of each component are presented in Tables 2 and 3, respectively. (A colour version of this figure is available in the online journal.)

where the ejecta from the WD envelope engulf the secondary star within a matter of minutes following outburst. The secondary transfers energy and angular momentum to the ejecta (Livio et al. 1990; Lloyd et al. 1997; Porter et al. 1998). WD rotation, when incorporated into calculations of the common-envelope phase, produces the observed prolate remnants (Porter et al. 1998).

#### 4.1 Model Assumptions

It is desirable when dealing with modelling to reduce computing time and yet have a physically sound model. The modelling of permitted line profiles so early after outburst is complicated by the fact that they are most likely affected by an optically thick medium. The full treatment of radiative transfer requires full knowledge of several parameters of the system and further assumptions are required. For example, the temperature of the central system in outburst, which can be derived from multi-frequency observations, and the density of each component, which is much harder to derive since we must assume an ejected mass and a geometry of the system.

We considered the effects of radiative transfer on the line profile and found that the the lower the inclination the more the ab-

<sup>2</sup> Available from <http://bufadora.astrosen.unam.mx/shape/>

**Table 3.** Derived FWHM velocity for each of the 5 components of the H $\alpha$  line in V2491 Cyg (see Fig. 3 and text for details).

Date	days after outburst	Component FWHM Velocity (km s <sup>-1</sup> )				
		1	2	3	4	5
2008 April 16	5	1729±47	1357±24	1870±3487	1379±130	1166±91
2008 April 19	8	1664±48	1412±14	1807±1780	1429±109	1115±41
2008 April 20	9	1649±40	1399±101	1998±1222	1488±57	1050±27
2008 April 21	10	1658±101	1239±53	1995±2238	1261±137	1194±74
2008 April 22	11	1660±89	1283±59	2694±2978	1305±137	1084±53
2008 April 23	12	1639±180	1384±210	1617±776	1476±395	1030±167
2008 April 24	13	1421±110	1335±83	1765±2077	1364±169	1127±92
2008 May 03	22	1340±60	910±27	931±86	1502±105	806±40
2008 May 06	25	1232±255	996±236	1081±678	1477±382	875±63
2008 May 12	31	1189±103	1096±76	1725±298	1832±324	795±26

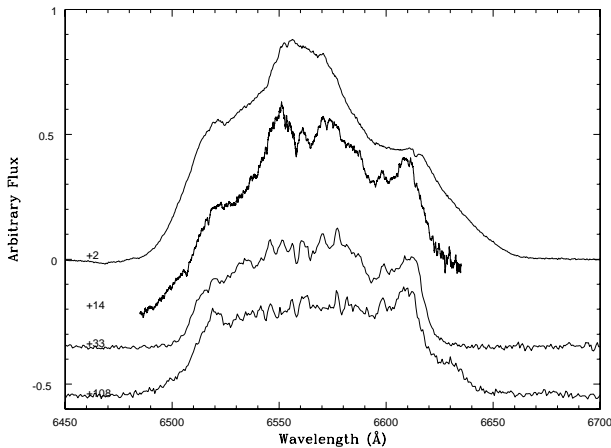


**Figure 4.** Spectral evolution of the high resolution H $\alpha$  line profile from several telescopes as shown in Table 1 and in the text. The spectra has been offset and the numbers on the left are days after outburst.

sorption affects the system but the overall line shape does not significantly change from the optically thin case. Furthermore, the absorption affects more the lower velocity systems. So when dealing with the results caution is necessary especially with the densities derived from the models because applying a density in the optically thin case will actually be only a lower limit to the true density of a system with greater opacity.

We also made the assumption that at early times the structures are still volume filled. della Valle et al. (2002) have shown the H $\alpha$  spectral evolution of V382 Vel from early outburst to the nebular stage (5 to 498 days after outburst); at early stages the line profile showed an asymmetric saddle-shape with the blue component more prominent than the red. The blue component diminishes in strength and the whole line profile develops to become a flat-topped shape. They associate this with the termination of the post-outburst wind phase and the complete ejection of the envelope. Our higher resolution spectra, Fig. 4, also show a similar development, and a similar interpretation can be made here.

#### 4.2 Model Parameters

Given V2491 Cyg’s fast decline from maximum we assume an axial ratio of 1.15 for our chosen structures following the relationships in Slavin et al. (1995). We also consider the possibility of a structure similar to RS Oph, first coined “peanut-shaped”

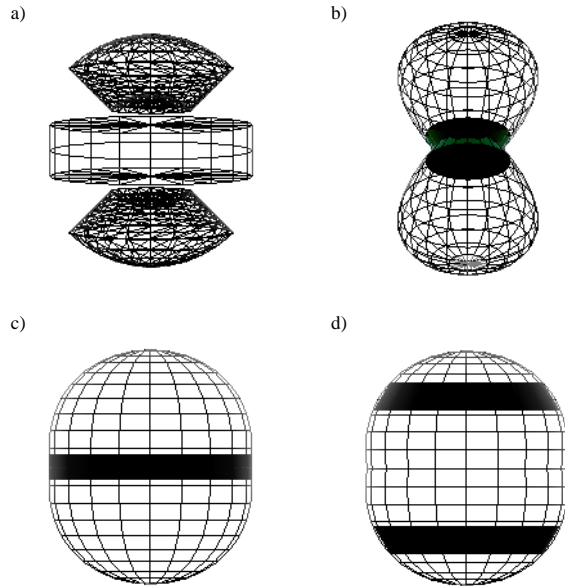


**Figure 5.** Models as visualised in SHAPE. a) polar blobs with an equatorial ring (Model A), b) a dumbbell structure with an hour-glass overdensity (Model B), c) prolate shell with an equatorial ring (Model C) and d) prolate shell with tropical rings (Model D).

(Bode et al. 2007) and later modelled as a dumbbell structure with an hour-glass-shaped central overdensity (Ribeiro et al. 2009). This model is included in our studies because, as mentioned before, this system has been suggested as a RN and a similar structure has been proposed for the RN U Sco (Drake & Orlando 2010). The candidate structures we chose are (i) polar blobs with an equatorial ring (Model A, e.g., HR Del; Hutchings 1972; Solf 1983); (ii) a dumbbell with an inner hour-glass overdensity with an axial ratio the same as derived above for RS Oph (Model B); (iii) prolate shell with an equatorial ring (Model C); and (iv) a prolate shell with tropical rings (Model D, e.g., V705 Cas; Gill & O’Brien 1999). As noted above, Model B differs from that generated by the common-envelope phase described above because the observed structure could arise due to interaction with a pre-existing red-giant wind and/or collimation by the accretion disc (e.g., Bode et al. 2007; Sokoloski et al. 2008; Ribeiro et al. 2009). Our models, as visualised in SHAPE, are shown in Fig. 5.

The lack of a resolved image of the remnant means any model

is not as well constrained as when the structure is spatially resolved. However, for the models assumed above we constrain a system inclination (where an inclination  $i = 90$  degrees corresponds to the orbital plane being edge-on, and  $i = 0$  degrees being face-on) and an expansion assumed to take place in a Hubble flow.

We explore the parameter space from 0–90 degrees and maximum expansion velocity ( $V_{\text{exp}}$ ) ranging from 100–8000 km s<sup>-1</sup> (in steps of 1 degree and 100 km s<sup>-1</sup>, respectively). We exclude  $V_{\text{exp}} > 8000$  km s<sup>-1</sup> as this is much higher than those normally associated with novae and indeed is at the lower end of velocities found in Type Ia Supernovae (e.g., Livio 2000). We note here however, that in the helium nova V445 Pup high speed knots were observed moving at  $8450 \pm 570$  km s<sup>-1</sup> (Woudt et al. 2009). The models were run several times to produce a well sampled model spectrum. The model spectra are compared to the observed spectra and flux matched via  $\chi^2$  minimisation, using techniques from Press et al. (1992). Furthermore, an estimate of the density ratio of each component was derived from their total fluxes using the task `SPECTFIT` in IRAF<sup>3</sup>. These were used as inputs for the relative structure densities.

## 5 MODELLING RESULTS

### 5.1 First epoch observations at $t = 25$ days after outburst

Shown in Fig. 6 are the results of our model fits, and their respective  $1\sigma$  errors, for all the model runs. Panel a) shows the results for Model A. These suggest that the best fit for this model is an inclination of  $80^{+3}_{-12}$  degrees with  $V_{\text{exp}}$  for the polar blobs of  $\sim 3100^{+200}_{-100}$  km s<sup>-1</sup> and for the equatorial ring of  $\sim 2700^{+200}_{-100}$  km s<sup>-1</sup>. The individual component fluxes are about the same. Panel b) shows the results for Model B. These suggest that the best fit to the model is for a system with inclination  $63^{+23}_{-8}$  degrees and  $V_{\text{exp}}$  of  $3500 \pm^{+1500}_{-300}$  km s<sup>-1</sup>. The flux is dominated by the dumbbell component. Panel c) shows the results for Model C. These suggest that the best fit to the model is for a system with inclination  $50^{+33}_{-12}$  degrees and  $V_{\text{exp}}$  of  $2800^{+300}_{-200}$  km s<sup>-1</sup>. The flux is dominated by the prolate structure. Finally, panel d) shows the results for Model D. These suggest that the best fit to the model is for a system with inclination  $54^{+36}_{-21}$  degrees and  $V_{\text{exp}}$  of  $2800^{+300}_{-200}$  km s<sup>-1</sup>. The flux is again dominated by the prolate structure.

As previously mentioned these results are not as well constrained as they would be if we could have the spectra combined with imaging data. We also performed modelling for a simple sphere. The results suggest that the best fit maximum expansion velocity  $V_{\text{exp}} \sim 2700$  km s<sup>-1</sup>. The shape of the synthetic spectra was that of an inverted U (similar to the prolate components in Models C and D of Fig. 6).

To determine the best fitting morphology we examined the derived reduced  $\chi^2$  probabilities and found that Models A and B showed comparable probabilities. The other structures gave negligible probabilities.

### 5.2 Second epoch observations at $t = 108$ days after outburst

Another test we perform on our models to see which best reproduces the data, considering only Models A and B, is to evolve

the models to a later epoch, keeping the parameters for inclination and  $V_{\text{exp}}$  as derived from the first epoch to the second epoch. In the case of Model A, it was allowed to evolve linearly. However, Ribeiro et al. (2009) suggested that their central component for RS Oph showed deceleration and we therefore kept this central component the same size from one epoch to the next in Model B.

What is evident is that if the models are allowed to evolve linearly, with the derived parameters the same, then the line profile should look identical from one epoch to the next in the absence of other physical changes. For the line profile to change, but with the velocity field and inclination constant, there must be a transition involving other factors. Just changing the densities does not suffice without the addition of new components. This transition may therefore be associated to the termination of the post-outburst wind phase and the complete ejection of the envelope, which is proposed to happen within the first couple of weeks (as in V382 Vel; della Valle et al. 2002). Therefore, the later epoch modelling does not have a filled distribution but now has a depth of material (shell) determined by the first epoch model. We therefore apply a volume distribution within this shell to both models and compare with the spectrum at day 108 after outburst (Fig. 4). Furthermore, Munari et al. (2010b) from photo-ionisation models showed the nova to be in the nebular stage at day 108 after outburst and the [N II] 6548 and 6584 Å emission lines may contribute significantly to the H $\alpha$  profile. Certainly [O III] was about ten times stronger than H $\alpha$  at this time (see Table 4 in Munari et al. 2010b).

#### 5.2.1 Model B – Dumbbell with an hour-glass overdensity

We do not show the Model B synthetic spectrum as it did not reproduce the observed second epoch spectrum at all well. The synthetic spectrum was that of an upside down “T” shape. We therefore, believe that Model A is the correct model for V2491 Cyg.

#### 5.2.2 Model A – Polar blobs and equatorial ring

In light of the presence of [N II] we should account for this when modelling the spectra on day 108. We should expect [N II] to appear as the expanding remnant becomes less dense overall and the nebular spectrum emerges. In the first instance, to fit the observed spectrum the velocities were kept constant from the first epoch for the H $\alpha$  and [N II] lines and only the relative flux was allowed to change. We assume here that the model derived for H $\alpha$  is the same for [N II]. This did not reproduce the observed spectrum without introducing significant additional absorption features.

We therefore allowed the velocity of the different components to change keeping the flux ratio of the [N II] lines always at 1:3 and the relative flux of the H $\alpha$  to the [N II] lines as a free parameter. The result of this modelling is shown in Fig. 7. This provides an excellent fit to the spectrum at day 108. The derived velocities for the polar blobs were  $\sim 3500$  km s<sup>-1</sup> (H $\alpha$ ) and  $\sim 3600$  km s<sup>-1</sup> ([N II]) and for the equatorial ring  $\sim 2700$  km s<sup>-1</sup> (H $\alpha$ ) and  $\sim 2600$  km s<sup>-1</sup> ([N II]). These results are within  $2\sigma$  of those derived for the first epoch.

It should be noted that there is a change in the contributions to the flux of the different components of H $\alpha$ . Where in the first epoch the two components were of comparable flux, in the second epoch the ring is the major contributor to the flux with relative flux contribution of the polar blobs to the ring of 1:2.5 for H $\alpha$ . This change in relative flux can be easily understood as arising from the fact that material moving at higher velocities will fade faster

<sup>3</sup> IRAF is distributed by the National Optical Astronomical Observatories, which is operated by the Associated Universities for Research in Astronomy, Inc., under contract to the National Science Foundation.

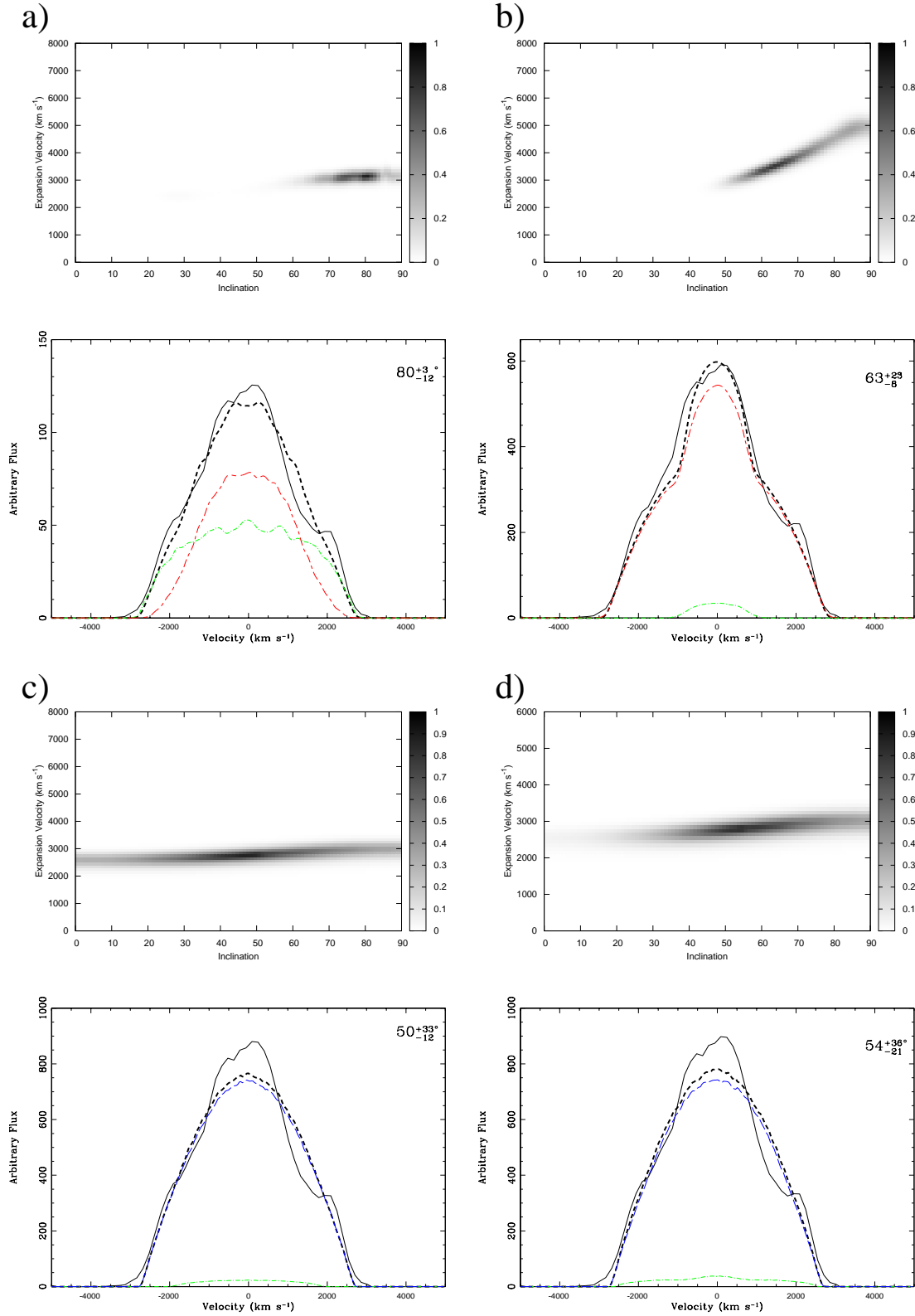


**Figure 6.** Results of the best fit model spectrum to the observed spectrum on day 25 after outburst. The images are for a) polar blobs with an equatorial ring (Model A), b) dumbbell structure with an hour-glass overdensity (Model B), c) prolate shell with an equatorial ring (Model C) and d) prolate shell with tropical rings (Model D). Displays, top – the most likely result for the structure, where the colour gradient represents the probability that the observed  $\chi^2$  value is correct. Bottom – the observed (solid black) and modelled spectrum (short-dash black). Also shown are the individual component contributions; rings (dot-dash green), prolate (long-dash blue) and polar blobs and dumbbell (short-dash-long-dash red). (A colour version of this figure is available in the online journal.)

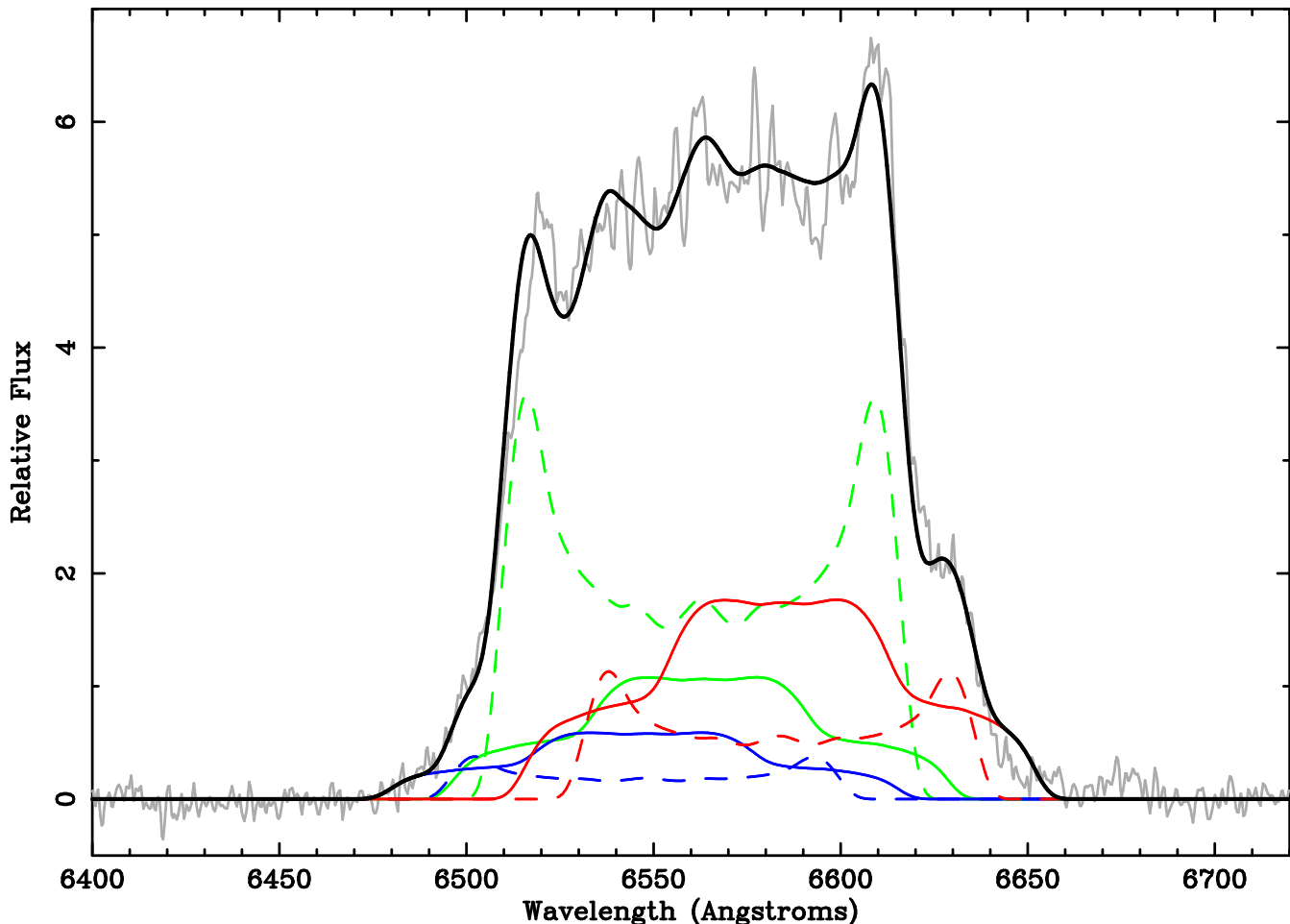


**Figure 7.** Fit to the observed line profile (grey) at day 108 after outburst. The model spectrum (black) is the sum of the individual components, H $\alpha$  (green), [N II] 6584Å (red) and [N II] 6548Å (blue). The ring (dashed line) and polar blobs (solid line). The ratio of the [N II] lines was kept at 1:3 and the relative flux of H $\alpha$  to the [N II] lines was kept as a free parameter. (A colour version of this figure is available in the online journal.)

in H $\alpha$  emission. Therefore, the change shown in Fig. 7, where the equatorial ring becomes the dominant component stems from the fact that it presents an expansion velocity lower than that of the polar blobs.

In the case of the [N II] line the polar blobs to ring relative flux contribution is 2.2:1. Their expansion velocities are  $\sim 3600$  km s $^{-1}$  and  $\sim 2600$  km s $^{-1}$ , respectively. We should also note that Munari et al. (2010b, their Figure 10) show a line profile at day 477 which is very different from the day 108 line profile. It does not have a flat top profile and has significant asymmetry. Our model can also account for this if the densities of the different components continue to evolve. As the nebula becomes less dense we expect that the relative contribution from [N II] should increase.

There is one more test we can perform to further constrain our model. The derived inclination of 80 degrees is very high and we therefore expect eclipses whose existence we are now investigating. Such eclipses should be easily observed in this system. For example, the CN DQ Her (orbital period  $\sim 4$  h) shows deep  $\sim 0.9$  mag eclipses in UBV $R$  (Zhang et al. 1995) as does the RN U Sco with eclipses of depth  $\sim 1.5$  mag in B (Schaefer & Ringwald 1995). Of course, if V2491 Cyg turns out to be eclipsing this will also enable us to determine more precisely important parameters of the central binary.

## 6 DISCUSSION AND CONCLUSIONS

Of the morphologies discussed above early in outburst, Models A and B, are the best fitting and give results that are very similar to each other early in outburst and this is reflected on the fact that the inclinations of the two morphologies overlap, within the errors. Furthermore, the main real difference is in the size of the central region. Model A is representative of a CN system, while the Model B has a morphology that has been observed in the RN RS Oph.

To model the second epoch observations the model was allowed to evolve into a system that was not volume filling but a shell. To replicate the observed spectrum with Model A at this time we needed to introduce significant emission from the [N II] lines and the components densities required to be changed with the equatorial ring becoming the dominant contributor to the flux. The change in derived densities between the components should also be expected since the different components are moving at different speeds. Emission from the polar blobs moving at higher speed will be observed to fade faster than the equatorial ring. Model B at the second epoch did not reproduce the line profile. Therefore, from the second epoch observations we suggest that Model A is the most likely with an inclination of  $80_{-12}^{+3}$  degrees and a maximum expansion velocity of  $3100_{-100}^{+200}$  km s $^{-1}$ , for the polar blobs. This velocity

is in line with those found in high-ionisation absorption lines in X-ray spectra by Ness et al. (2010).

The high inclination found for Model A is however difficult to reconcile with the outburst amplitude vs. decline rate relationship for classical novae (Warner 1987). The observed amplitude of 10 mags is much lower than that predicted for the derived inclination of 80 degrees (15.5 mags) while a pole-on system would still have a predicted amplitude of 12.5 mags. However, we note that RNe present a similar outburst amplitude at a similar inclination (e.g. Munari et al. 1999). This is in line with the suggested RN nature of this object from other authors (e.g., Page et al. 2010). Further exploration of the nature of the progenitor will be presented in Darnley et al. (2010).

#### ACKNOWLEDGMENTS

The authors are grateful to W. Steffen and N. Koning for valuable discussions on the use of *SHAPE* and adding special features to the code, N. Clay and C. Mottram for useful discussions on programming, Alessandro Siviero, Paolo Valisa and Lina Tomasella for assisting in collecting the spectra in Asiago, Witold Maciejewski for discussion on radiative transfer and Chris Collins for discussions on statistics. VARMR is funded by an STFC studentship. The Liverpool Telescope is operated on the island of La Palma by Liverpool John Moores University in the Spanish Observatorio del Roque de los Muchachos of the Instituto de Astrofísica de Canarias with financial support from the STFC. We thank an anonymous referee for valuable comments on the original manuscript.

#### REFERENCES

Ayani K., Matsumoto K., 2008, Central Bureau Electronic Telegrams, 1334  
Baklanov A., Pavlenko E., Berezina E., 2008, The Astronomer's Telegram, 1514  
Bode M. F., 2002, in Hernanz M., José J., eds, Classical Nova Explosions Vol. 637 of American Institute of Physics Conference Series, p. 497  
Bode M. F., 2010, AN, 331, 160  
Bode M. F., Evans A., 2008, Classical Novae, Cambridge Astrophysics Series, No. 43. Cambridge Univ. Press, Cambridge  
Bode M. F., Harman D. J., O'Brien T. J., Bond H. E., Starrfield S., Darnley M. J., Evans A., Eyres S. P. S., 2007, ApJ Let., 665, L63  
Bode M. F., Darnley M. J., Shafter A. W., Page K. L., Smirnova O., Anupama G. C., Hilton T., 2009, ApJ, 705, 1056  
Boehm-Vitense E., 1981, ARA&A, 19, 295  
Brandi E., Quiroga C., Mikołajewska J., Ferrer O. E., García L. G., 2009, A&A, 497, 815  
Darnley M. J., Ribeiro V. A. R. M., Bode M. F., Munari U., 2010, A&A, submitted  
della Valle M., Pasquini L., Daou D., Williams R. E., 2002, A&A, 390, 155  
Drake J. J., Orlando S., 2010, ApJ, 720, L195  
Dobrzycka D., Kenyon S. J., 1994, AJ, 108, 2259  
Fekel F. C., Joyce R. R., Hinkle K. H., Skrutskie M. F., 2000, AJ, 119, 1375  
Gill C. D., O'Brien T. J., 1999, MNRAS, 307, 677  
Hachisu I., Kato M., 2009, ApJ Let., 694, L103

Hachisu I., Kato M., Kato T., Matsumoto K., 2002, in Gänsicke B. T., Beuermann K., Reinsch K., eds, The Physics of Cataclysmic Variables and Related Objects Vol. 261 of Astronomical Society of the Pacific Conference Series, p. 629  
Henden A., Munari U., 2008, Information Bulletin on Variable Stars, 5834  
Hernanz M., Sala G., 2002, Science, 298, 393  
Hutchings J. B., 1972, MNRAS, 158, 177  
Ibarra A., Kuulkers E., 2008, The Astronomer's Telegram, 1473  
Ibarra A., et al., 2008, The Astronomer's Telegram, 1478  
Ibarra A., et al., 2009, A&A, 497, L5  
Jurdana-Sepic R., Munari U., 2008, IBVS, 5839  
King A. R., Watson M. G., 1987, MNRAS, 227, 205  
King A. R., Whitehurst R., Frank J., 1990, MNRAS, 244, 731  
Livio M., 2000, in J. C. Niemeyer & J. W. Truran ed., Type Ia Supernovae, Theory and Cosmology p. 33  
Livio M., Shankar A., Burkert A., Truran J. W., 1990, ApJ, 356, 250  
Lloyd H. M., O'Brien T. J., Bode M. F., 1997, MNRAS, 284, 137  
Munari U., et al., 1999, A&A, 347, L39  
Munari U., Ribeiro V. A. R. M., Bode M. F., Saguner T., 2010a, MNRAS, in press  
Munari U., Siviero A., Dallaporta S., Cherini G., Valisa P., Tomasella L., 2010b, New Astron., in press  
Naik S., Banerjee D. P. K., Ashok N. M., 2009, MNRAS, 394, 1551  
Nakano S., et al., 2008, IAU Circ., 8934  
Ness J.-U., et al., 2010, ApJ, submitted  
O'Brien T. J., Bode M. F., 2008, in Bode M. F., Evans A., eds, Classical Novae Vol. 43 of Cambridge: Cambridge University Press, p. 285  
Page K. L., et al., 2010, MNRAS, 401, 121  
Pagnotta A., Schaefer B. E., Xiao L., Collazzi A. C., Kroll P., 2009, AJ, 138, 1230  
Porter J. M., O'Brien T. J., Bode M. F., 1998, MNRAS, 296, 943  
Press W. H., Teukolsky S. A., Vetterling W. T., Flannery B. P., 1992, Numerical recipes in C. The art of scientific computing  
Ribeiro V. A. R. M., et al. 2009, ApJ, 703, 1955  
Schaefer B. E., Ringwald F. A., 1995, ApJ, 447, L45  
Slavin A. J., O'Brien T. J., Dunlop J. S., 1995, MNRAS, 276, 353  
Sokoloski J. L., Rupen M. P., Mioduszewski A. J., 2008, ApJ Let., 685, L137  
Solf J., 1983, ApJ, 273, 647  
Starrfield S., Sparks W. M., Truran J. W., 1985, ApJ, 291, 136  
Steele I. A., et al., 2004, SPIE, 5489, 679  
Steffen W., López J. A., 2006, Revista Mexicana de Astronomia y Astrofísica, 42, 99  
Steffen W., Koning N., Wenger S., Morisset C., Magnor M., 2010, preprint (arXiv:1003.2012)  
Warner B., 1987, MNRAS, 227, 23  
Williams R. E., Hamuy M., Phillips M. M., Heathcote S. R., Wells L., Navarrete M., 1991, ApJ, 376, 721  
Woudt P. A., et al., 2009, ApJ, 706, 738  
Yaron O., Prialnik D., Shara M. M., Kovetz A., 2005, ApJ, 623, 398  
Zhang E., Robinson E. L., Stiening R. F., Horne K., 1995, ApJ, 454, 447